

# Dimer motion on a periodic substrate: Spontaneous symmetry breaking and absolute negative mobility

David Speer<sup>1</sup>, Ralf Eichhorn<sup>2</sup>, Mykhaylo Evstigneev<sup>1</sup>, and Peter Reimann<sup>1</sup>

<sup>1</sup>*Universität Bielefeld, Fakultät für Physik, 33615 Bielefeld, Germany*

<sup>2</sup>*NORDITA, Roslagstullsbacken 23, 10691 Stockholm, Sweden*

We consider two coupled particles moving along a periodic substrate potential with negligible inertia effects (overdamped limit). Even when the particles are identical and the substrate spatially symmetric, a sinusoidal external driving of appropriate amplitude and frequency may lead to spontaneous symmetry breaking in the form of a permanent directed motion of the dimer. Thermal noise restores ergodicity and thus zero net velocity, but entails arbitrarily fast diffusion of the dimer for sufficiently weak noise. Moreover, upon application of a static bias force, the dimer exhibits a motion opposite to that force (absolute negative mobility). The key requirement for all these effects is a non-convex interaction potential of the two particles.

PACS numbers: 05.45.-a, 05.40.-a, 05.60.-k

## I. INTRODUCTION

The dynamics of a dimer in the presence of a periodic potential is of interest in a variety of different contexts. A first example is a diatomic molecule adsorbed and moving on a crystal surface [1–3], e.g. during crystal growth or thin film formation [4–7]. In many cases, the dimer is able to explore the entire two-dimensional surface, but in some cases also an effectively one-dimensional motion arises, e.g. due to a strong crystalline anisotropy, a pronounced step, or a channeled (110) metal surface [5, 7]. As an example, Fig. 1 illustrates a  $\text{Si}_2$  or  $\text{Ge}_2$  dimer confined between the rows of the reconstructed  $\text{Si}(001)$  or  $\text{Ge}(001)$  surface, see [8] and references therein. Motion of two coupled atoms (or defects, nanoparticles, etc.) in a three-dimensional (atomic, optical etc.) lattice is yet another option along these lines. Further important examples are simple models of processive molecular motors consisting of two elastically coupled “heads” (motor domains) and walking along a polymer filament [9–18]. Artificially manufactured set-ups include colloidal doublets [19] in periodic arrays of magnetic [20] or optical [21] traps. Last but not least, dimer models are well established to describe the sliding friction of two coupled asperities at the nanoscale [22–25], but also arise in less “obvious” systems like superionic conductors [26], dissociated dislocations [27], and SQUIDS [28, 29].

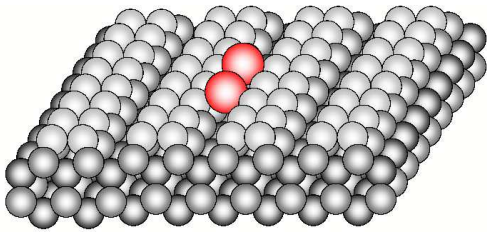


FIG. 1: (Color online): Schematic illustration of the confined motion of a  $\text{Si}_2$  or  $\text{Ge}_2$  dimer (big red spheres) within the rows of a  $2 \times 1$  reconstructed  $\text{Si}(001)$  or  $\text{Ge}(001)$  surface (small grey spheres).

In most of the previous theoretical studies, the dimer was driven out of equilibrium by some external forcing and the spatial inversion symmetry of the system was broken a priori in one or another way. Most prominently, in the context of so called ratchet effects, a spatial anisotropy of either the substrate potential or of the dimer itself was assumed [9, 11, 13–17, 30–47]. Another important direction concerns the behavior of drift and diffusion when the spatial symmetry is broken by an externally applied, constant “bias”-force [6, 23, 27, 48, 49]. Studies of fully symmetric dimer models have focused on the diffusive properties, since a systematic directed dimer motion seems – at first glance “obviously” – not possible in such systems [1, 3, 4, 7, 8, 24, 50]. Exceptions are some idealized conservative (Hamiltonian) models [5, 51] and the recent paper [52], to which we come back in Sec. X.

In our present study, the main focus is on dimers consisting of identical particles and on spatially periodic systems without any intrinsically broken symmetry. To avoid unnecessary complications, we furthermore assume that inertia effects are negligible (overdamped limit) [9, 11, 13–17, 30–33, 35, 36, 39, 40, 42–48], and that the dimer is driven out of equilibrium by a sinusoidally oscillating force [31–33, 36, 37, 39, 42, 52, 53]. Our first main result will be that – in spite of the spatial symmetry of the system – the deterministic dynamics still admits a systematic net motion of the dimer via spontaneous symmetry breaking. In particular, ergodicity is broken, and thus the direction of the spontaneous transport depends on the initial conditions. Upon including thermal noise, ergodicity is restored, and thus the average dimer velocity must be zero. But now – quasi as a precursor of the spontaneous deterministic transport – the diffusion coefficient diverges for asymptotically weak noise. Finally, we will demonstrate that upon application of a static bias force, the system may respond with motion opposite to that force, i.e. it exhibits so-called absolute negative mobility. The main and indispensable prerequisite for all these effects is a non-convex interaction potential of the two particles. This quite unexpected

and remarkable condition also seems to explain why such effects have not been “accidentally” discovered in previous studies of overdamped dimer motion. An exception is the recent absolute negative mobility effect in Ref. [29] which will be discussed in more detail in Sec. X.

## II. ONE-DIMENSIONAL MODEL

With the exception of Sec. IX, we will always focus on the one-dimensional motion of two coupled, identical particles with coordinates  $x_i$  ( $i = 1, 2$ ), modeled by the Langevin equations

$$\eta \dot{x}_i(t) = -\frac{\partial U_{tot}(x_1(t), x_2(t))}{\partial x_i} + F + f(t) + \xi_i(t) . \quad (1)$$

In doing so, inertia terms  $m\ddot{x}_i(t)$  are considered as negligible (overdamped limit),  $\eta$  is the viscous friction (damping) coefficient of the single particles, and  $F$  a static “bias”-force. Furthermore,  $f(t)$  represents an external driving with time period  $\tau$ , satisfying the symmetry condition

$$f(t + \tau/2) = -f(t) , \quad (2)$$

and thermal fluctuations are modeled by independent Gaussian noises  $\xi_i(t)$  of zero mean and respecting the fluctuation-dissipation relation

$$\langle \xi_i(t) \xi_j(s) \rangle = 2 \eta k_B T \delta_{ij} \delta(t - s) , \quad (3)$$

where  $k_B$  is Boltzmann’s constant and  $T$  the ambient temperature. The potential energy  $U_{tot}(x_1, x_2)$  is of the form

$$U_{tot}(x_1, x_2) = U(x_1) + U(x_2) + W(x_1 - x_2) \quad (4)$$

with a *spatially symmetric* and  $L$ -periodic single-particle potential  $U(x)$  and an interaction potential  $W(y)$  which will be further specified later on.

For the sake of convenience, we will often adopt units of time, length, temperature, and energy so that

$$\eta = 1, \quad L = 2\pi, \quad k_B = 1, \quad \max_x U(x) - \min_x U(x) = 2 . \quad (5)$$

When specific examples will be needed, we will furthermore focus on

$$U(x) = \cos(x) \quad (6)$$

$$f(t) = A \sin(\omega t) \quad (7)$$

with  $\omega := 2\pi/\tau$ , and either a Lennard-Jones or a quartic interaction potential of the form (see also Fig. 2)

$$W(y) = (\lambda/y)^{12} - 2(\lambda/y)^6 , \quad (8)$$

$$W(y) = c(y - \Delta)^3(y - \Delta - 2) , \quad (9)$$

with positive parameters  $c, \lambda, \Delta$ . We expect and explicitly verified in a few cases that a large variety of similar

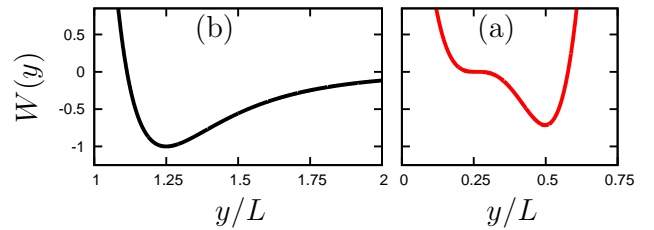


FIG. 2: (Color online) (a) The Lennard-Jones interaction potential (8) for  $\lambda = 1.25 L$ . (b) The quartic interaction potential (9) for  $c = 0.428$  and  $\Delta = 0.26 L$  (see also Fig. 3).

potentials  $U(x)$ ,  $W(y)$  and forces  $f(t)$  lead to qualitatively unchanged results (see also Secs. VI and IX).

The Lennard-Jones potential (8) is a well established prototype model for the interaction of atoms. In our present context, it has the only, and mainly puristic, shortcoming that for any finite thermal noise, a dimer ultimately dissociates after sufficiently long time into two separate monomers. Our second example (9) is free of this problem and, moreover, exhibits a slightly richer “intra-well” structure of the potential landscape, see Fig. 2. In particular, it has a metastable inflection point at  $y = \Delta$ , thus mediating between a “purely” monostable and a “genuine” bistable interaction potential. We thus can expect that the results we will find for (9) are still qualitatively recovered for suitable monostable as well as bistable interaction potentials (see Sec. VI.C).

Note that interaction potentials in real systems are expected to satisfy the symmetry  $W(-y) = W(y)$ . In contrast, we also admit non-symmetric  $W(y)$ , e.g. in (9), for the mere sake of convenience later on. However, when dealing with asymmetric  $W(y)$ , we tacitly restrict ourselves to cases for which a change of sign of  $x_1 - x_2$  in (4) is a negligibly rare event in the dynamics (1), e.g. by admitting only sufficiently large  $c$ -values in (9). In other words, the two monomers do not pass each other in practice, and thus only  $y$ -values of one sign, say  $y > 0$ , actually matter in  $W(y)$ .

Later on, our main focus will be on non-convex interaction potentials  $W(y)$ . Various physical realizations of such potentials will be discussed in Sec. V. Depending on the particular system, the external driving forces  $F$  and  $f(t)$  may be realized by hydrodynamic flows, traveling optical potentials, electrical fields, magnetic fields, or mechanical agitation.

## III. BASIC NOTIONS

Given the model (1)-(4), it is natural to go over to center of mass and relative coordinates

$$x := (x_1 + x_2)/2 , \quad y := x_1 - x_2 . \quad (10)$$

In the special case (5)-(7), their equations of motion take the form

$$\dot{x}(t) = \sin(x) \cos(y/2) + A \sin(\omega t) + F + \sqrt{T} \tilde{\xi}_1(t) \quad (11)$$

$$\dot{y}(t) = 2 \cos(x) \sin(y/2) - 2W'(y) + 2\sqrt{T} \tilde{\xi}_2(t) \quad (12)$$

where  $\tilde{\xi}_{1,2}(t)$  are independent, delta-correlated Gaussian noises.

A first main quantity of interest is the time averaged velocity of the dimer's center of mass,

$$v := \frac{\tau}{L} \lim_{t \rightarrow \infty} \frac{1}{t} \int_0^t dt' \dot{x}(t'), \quad (13)$$

expressed as a dimensionless multiple of the spatial and temporal periods  $L$  and  $\tau = 2\pi/\omega$  for reasons of convenience later on.

For any finite noise strength  $T$ , the dynamics (1) is ergodic, i.e. the velocity (13) is (with probability one) equal to the ensemble averaged velocity. In particular, the velocity is independent of the initial conditions  $x_i(0)$  and of the realization of the noise  $\xi_i(t)$ .

In contrast, in the deterministic limit ( $T = 0$ ), the velocity (13) may – as we will see later – still depend on the initial conditions  $x_i(0)$ , implying that ergodicity of the dynamics (1) is broken.

A second quantity of interest is the diffusion coefficient of the dimer's center of mass,

$$D := \lim_{t \rightarrow \infty} \frac{\langle x^2(t) \rangle - \langle x(t) \rangle^2}{2t}, \quad (14)$$

where  $\langle \cdot \rangle$  indicates an ensemble average over different realizations of the noise  $\xi_i(t)$ . For any  $T > 0$ , ergodicity implies that an additional averaging over different initial condition  $x_i(0)$  is possible but actually superfluous in (14).

Next, we turn to the notion of spontaneous symmetry breaking. Generally speaking, this notion refers to a description (model) of a system in terms of some mathematical equations which exhibit a certain symmetry (invariance), while their solutions (system states) do not exhibit this symmetry. The simplest example is the equations

$$a + b = 1, \quad ab = 0 \quad (15)$$

which are clearly symmetric in  $a$  and  $b$ , while their solutions, namely  $(a, b) = (1, 0)$  and  $(a, b) = (0, 1)$ , both break this symmetry. It also exemplifies the general rule that different symmetry breaking solutions are related to each other via the original system symmetry. The simplest physical example is tossing a coin, illustrating that the decision about which state the system actually selects is usually rooted in the initial conditions and/or some “random effects”.

Returning to our dynamics (1)-(4), we observe that it satisfies the following basic symmetry property: If  $x_{1,2}(t)$  is a solution of (1) then – due to the symmetry of  $f(t)$  in (2) and of  $U(x)$  mentioned below (4) – also  $x_{1,2}^*(t) :=$

$-x_{2,1}(t + \tau/2)$  will be a solution of (1), provided  $F$  is replaced by  $-F$  and  $\xi_{1,2}(t)$  by  $\xi_{1,2}^*(t) := -\xi_{2,1}(t + \tau/2)$ .

For  $T = 0$  (deterministic limit) and  $F = 0$  (unbiased system) the dynamics (1)-(4) is thus – up to an irrelevant shift of the time-origin and a relabeling of the (identical) particles – symmetric under spatial inversion. It follows that for any possible value of the velocity  $v$  according to (13), also the opposite velocity  $v^* = -v$  occurs with the same probability (under the tacit assumption of an analogous equal a priori likelihood of the initial condition  $x_i(0)$  and  $x_i^*(0)$ ). Since, as mentioned above, different initial conditions indeed may lead to different velocities, it follows that our symmetric system may give rise to solutions which break the symmetry of the system by exhibiting a finite velocity in either one or the other direction. As usual (see above), we will refer to such a case as *spontaneous symmetry breaking* and to the concomitant dimer motion as *spontaneous transport*.

Turning to  $T > 0$  (and arbitrary  $F$ ), the above mentioned fact that the velocity  $v$  from (13) is independent of the initial conditions and the realization of the noise results in the basic symmetry property that  $F \mapsto -F$  implies  $v \mapsto -v$ .

In particular, in the unbiased case  $F = 0$  we recover  $v = 0$  for any  $T > 0$ . Regarding finite bias forces  $F$ , one could naively expect that the velocity (13) now should take on a finite value and that its sign should always correspond to that of  $F$ . The quite unexpected contrary behavior, namely a velocity  $v$  opposite to the applied force, is termed *absolute negative mobility* [54].

The main aim of our paper is to demonstrate that the dynamics (1) indeed may give rise to spontaneous transport and to absolute negative mobility, and that there exists in fact a close connection between these two quite astonishing effects. A comparison with related previous works is provided in Sec. X.

#### IV. NO-GO THEOREMS FOR CONVEX INTERACTION POTENTIALS

In this section we demonstrate that spontaneous transport and absolute negative mobility (as specified in the previous section) are ruled out for any dynamics (1)-(4) with a convex interaction potential  $W(y)$ , i.e.

$$W''(y) > 0 \text{ for all } y. \quad (16)$$

In order to exclude spontaneous transport, it is sufficient to demonstrate that the velocity (13) in the deterministic limit ( $T = 0$ ) is unique (independent of the initial conditions). Proceeding by way of a proof by contradiction, we assume that there exist two solutions of (1)-(4), called  $x_i(t)$  and  $x'_i(t)$ , with different velocities  $v$  and  $v'$  according to (13), say  $v' > v$  without loss of generality. Since for any integer  $n$ , also  $x_i(t) + nL$  solves (1)-(4) and yields the same velocity  $v$  in (13), we may without loss of generality assume that the initial conditions satisfy  $x_1(0), x_2(0) > x'_1(0), x'_2(0)$ . Since  $v' > v$ , the parti-

cles  $x'_i(t)$  must “catch up” with the particles  $x_i(t)$  in the course of time. Without loss of generality, the indices  $i$  can be chosen so that it is  $x'_1(t)$  which catches up with  $x_1(t)$  for the first time at some  $t = t^*$ , i.e.

$$x'_1(t^*) = x_1(t^*) \quad (17)$$

$$x'_2(t^*) \leq x_2(t^*) \quad (18)$$

$$\dot{x}'_1(t^*) \geq \dot{x}_1(t^*) . \quad (19)$$

The equality sign in (18) can be excluded, since otherwise (17) and the dynamics (1)-(4) (with  $T = 0$ ) would imply that  $x'_i(t) = x_i(t)$  for all  $t$ , and thus  $v' = v$ . With  $y := x_1(t^*) - x_2(t^*)$  and  $y' := x'_1(t^*) - x'_2(t^*)$  it follows that

$$y' > y , \quad (20)$$

and by introducing (17) into (1)-(4) (with  $T = 0$ ) we find

$$\dot{x}'_1(t^*) - \dot{x}_1(t^*) = -W'(y') + W'(y) . \quad (21)$$

In view of (20) and (16) we thus can infer that  $\dot{x}'_1(t^*) - \dot{x}_1(t^*) < 0$ , in contradiction to (19). This concludes our proof that spontaneous transport is excluded.

Next we analogously proof by contradiction that (16) rules out absolute negative mobility for the dynamics (1)-(4) with  $T > 0$ . We thus consider a solution  $x_i(t)$  of (1)-(4) with velocity  $v$  according to (13) and a second solution  $x'_i(t)$  with  $F'$  instead of  $F$  in (1) and a resulting velocity  $v'$ . Assuming absolute negative mobility, it follows that two such solutions must exist with the property that  $F' < F$  and  $v' > v$ . In particular, we can assume the same realization of the noise  $\xi_i(t)$  in (1) for  $x_i(t)$  and for  $x'_i(t)$ , since – as mentioned in Sec. III – the velocity (13) is independent of the realization of the noise. As before,  $x_1(0), x_2(0) > x'_1(0), x'_2(0)$  can be taken for granted without loss of generality and  $v' > v$  then implies the existence of a time point  $t^*$  with the properties (17)-(19). With  $y := x_1(t^*) - x_2(t^*)$  and  $y' := x'_1(t^*) - x'_2(t^*)$  it follows that

$$y' \geq y , \quad (22)$$

but, unlike before,  $y' = y$  cannot be excluded now. From (1)-(4) we can infer that

$$\dot{x}'_1(t^*) - \dot{x}_1(t^*) = -W'(y') + W'(y) + F' - F . \quad (23)$$

Combining (16) with (22) yields  $-W'(y') + W'(y) \leq 0$  and with  $F' < F$  it follows that  $\dot{x}'_1(t^*) - \dot{x}_1(t^*) < 0$ , in contradiction to (19). We thus have proven that absolute negative mobility is impossible.

We remark that the above arguments can be readily generalized to more than two and/or non-identical particles with convex nearest-neighbor interaction potentials. In particular, in the context of the Frenkel-Kontorova model, the so-called Middleton’s no passing rule has been proven along similar lines, see [55–59] and further references therein.

## V. NON-CONVEX INTERACTION POTENTIALS

Non-convex interaction potentials occur naturally in various situations: First, this is the case for many common models of basic molecular interactions [1–3], such as Lennard-Jones [67] (cf. (8)) or Morse potentials [8, 34]. Second, less basic but still bistable molecular interaction potentials arise, e.g., in the modeling of random walkers in motor proteins [9–18, 66], and have also been considered in dimer ratchet models [39, 42, 43, 45]. Third, more complex dimers may have several stable configurations, or the dissociation process may involve additional (fast) internal degrees of freedom that lead to a non-convex effective interaction potential, as considered theoretically e.g. in [53]. Experimentally, e.g. in [80] a water droplet was positioned on a periodic surface and its shape (internal degree of freedom) was periodically driven by externally applied electric fields. Lastly, a spatially one dimensional model may serve as an approximation for the full three-dimensional dynamics of the dimer. The main effects of the other degrees of freedom are incorporated into the “effective” interaction forces between the monomers, resulting in a more complex, non-convex structure of the potential (cf. Sec. IX).

## VI. SPONTANEOUS SYMMETRY BREAKING

We consider the dynamics (1)-(4) without bias ( $F = 0$ ) in the deterministic limit ( $T = 0$ ). We furthermore focus on non-convex interaction potentials  $W(y)$ , for instance (8), (9). Is it possible that a solution  $x_i(t)$  spontaneously breaks the spatial symmetry of the system and exhibits a finite velocity  $v$  according to Eq. (13)? While there seems to be no a priori reasons why not, the actual existence of such solutions appears to us quite astonishing nevertheless. In accordance with this intuitive expectation, their existence turns out to be indeed restricted to relatively small parameter regions in the deep non-linear regime, thus making any further progress by analytical means quite hopeless. Therefore, we focus on the discussion of our extensive numerical results in the first place and only a posteriori provide a simplified intuitive picture of what is going on.

### A. Numerical example

Figure 3 presents typical results for the quartic potential from (9) (see also Fig. 2b). For each depicted point (“pixel”) in Fig. 3, we have calculated the velocity according to (13) for 20 trajectories of length  $500\tau$  with randomly chosen initial conditions. To eliminate “transient” effects, we furthermore excluded an initial time-interval of length  $150\tau$  for each trajectory contained in the average in (13). The black “islands” indicate parameter regions where all initial conditions which we nu-



merically tried out ended up on periodic attractors exhibiting spontaneous symmetry breaking, i.e. a finite net velocity of the rational form  $v = \pm n/m$  with positive integers  $n, m$  in the specific dimensionless units from (13). We note that spontaneous symmetry breaking may occur also with other types of attractors, e.g. chaotic attractors which emerge from the periodic ones by period doubling cascades [63] and thus still carry a rational net velocity of the form  $v = \pm n/m$ . However, they are not visible in Fig. 3, as their parameter regions are extremely small. Furthermore, we found that the black islands in Fig. 3 are largely dominated by the velocities  $v = \pm 1$ . The light grey “sea” around the black islands indicates parameter regions without spontaneous symmetry breaking, i.e. all probed initial conditions exhibited a net velocity of  $v = 0$  (in fact, every trajectory  $x(t)$  remained bounded, and, in particular, did not exhibit deterministic diffusion). The quite small remaining regions in mid-dark grey indicate coexistence of solutions with  $v = \pm n/m$  (like in the black islands) and with  $v = 0$  (like in the light grey sea). The tiny (almost invisible) white regions and single pixels in Fig. 3 indicate that the dimer trajectory was neither bounded nor did it reach a periodic attractor within the maximal numerical simulation time of  $1000\tau$ . Since those parameter regions are so small, we will not consider them any further.

The negative parameter regimes (omitted in Fig. 3) are either unphysical (e.g.  $c$  in (9)), follow by symmetry (e.g.  $A$  and  $\omega$  in (11)), or by periodicity (e.g.  $\Delta$  in (9)). For all the remaining (non-negative) parameters outside the range plotted in Fig. 3, either only solutions with  $v = 0$  were obtained, or – in the case of large  $A$ -values – the continuation is qualitatively quite obvious. By changing the values of those parameters which are held fixed in each of the three plots in Fig. 3, also the shape and positions of the “black islands” change considerably. E.g., we have found that for every given  $0.001 < \omega < 2$  it is possible to adapt the remaining parameters so that spontaneous symmetry breaking is realized (even smaller  $\omega$ -values become numerically very expensive and have therefore not been investigated any further). From this viewpoint, the range of symmetry breaking parameters is actually not so small as a first glance on Fig. 3 may suggest.

## B. Basic mechanism

In order to illustrate the characteristic features of the dimer motion when the symmetry is spontaneously broken, we focus, as a typical example, on the parameter values of the driving indicated by the “+” symbol in Fig. 3a and on the specific interaction potential  $W(y)$  depicted in Fig. 2b. For these parameter values, two periodic attractors with net velocity  $v = \pm 1$  coexist, which break the symmetry of the underlying equations of motion (11), (12). Figure 4 collects 9 snapshots of the associated dynamical evolution of the dimer during one driving period  $\tau$  on the attractor with  $v = +1$ . At the

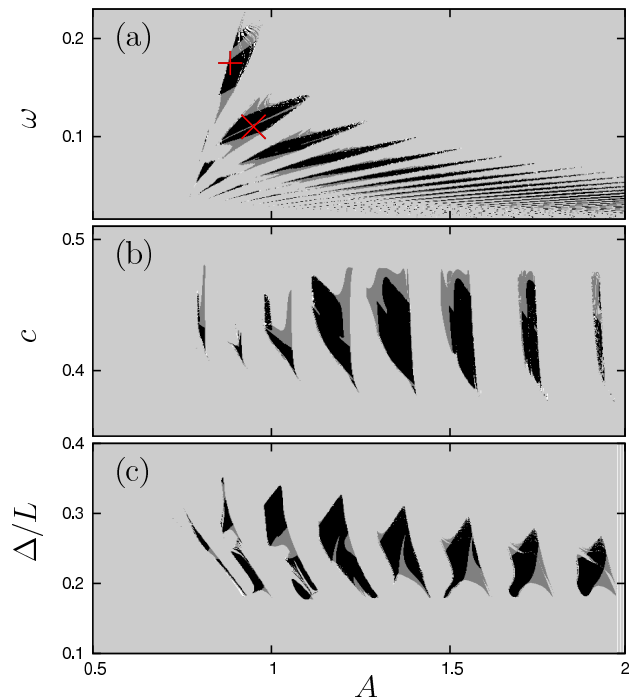


FIG. 3: (Color online) Velocity (13) obtained by numerically solving (11), (12) with  $F = 0$ ,  $T = 0$ , and (9) for various parameter values. (a) Variable driving amplitude  $A$  and frequency  $\omega$  with fixed parameters  $c = 0.428$ ,  $\Delta = 0.26L$  (these “odd” values are chosen on purpose to avoid all “accidental symmetries” or other sorts of “special cases”). The two crosses “+” and “x” indicate the specific parameter values adopted later in Fig. 4 and Fig. 6, respectively. (b) Variable driving amplitude  $A$  and interaction potential parameter  $c$  with fixed parameters  $\omega = 0.064$ ,  $\Delta = 0.26L$ . (c) Variable driving amplitude  $A$  and interaction potential parameter  $\Delta$  with fixed parameters  $\omega = 0.064$ ,  $c = 0.428$ . Black: Finite velocities  $v = \pm n/m$  with positive integers  $n$  and  $m$ . Light grey: Velocities  $v = 0$ . Intermediate grey: Coexistence of finite velocities  $v = \pm n/m$  and  $v = 0$ . For further details see main text.

beginning of the cycle, the dimer extension is close to its equilibrium value of  $y = L/2 = \pi$  (see also Fig. 2b and Eq. (5)). In this configuration, the forces due to the external periodic potential acting on the two particles are almost identical in modulus but have opposite signs, so that the center of mass motion of the dimer is practically not affected by the periodic potential (cf. Eq. (11) with  $y \approx L/2 = \pi$ ), whereas its impact on the relative coordinate  $y$  is maximal (cf. Eq. (12)). As a consequence, the dimer as a whole essentially follows the time-dependent driving force, while it is slightly stretched and compressed by the periodic potential landscape. This type of behavior can be observed in Fig. 4 during the first half of the driving period  $\tau$  and results in a displacement of the dimer’s center by a little more than one spatial period in the positive  $x$  direction. The deviations from the equilibrium length  $y = L/2$  are stabilized very quickly due to the convex character of the interaction potential

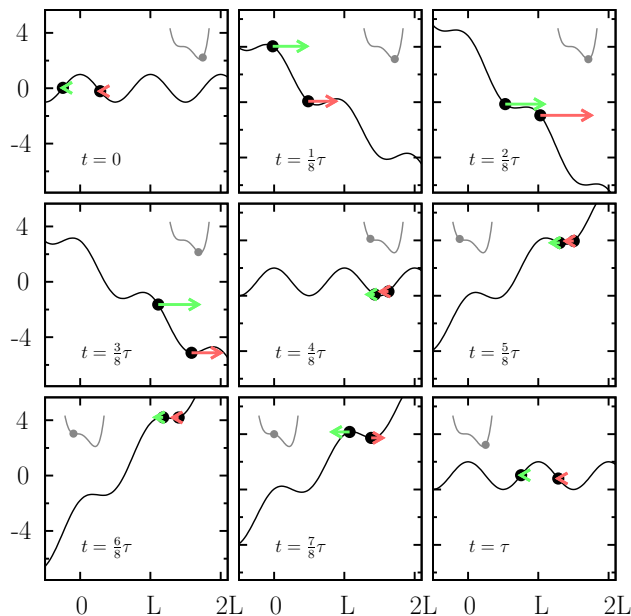


FIG. 4: (Color online) Time evolution of a typical spontaneous symmetry breaking periodic attractor of (11), (12) with interaction potential (9) and the specific parameter values indicated by the “+” symbol in Fig. 3a, i.e.  $\omega = 0.175$ ,  $A = 0.885$  and all remaining parameters as in Fig. 3a. The black dots indicate  $x_1(t)$  (right dot) and  $x_2(t)$  (left dot), the arrows  $\dot{x}_1(t)$  and  $\dot{x}_2(t)$ , and the black lines the tilted periodic potential  $U(x) - (x - L/2)f(t)$ . The dark grey “insets” indicate the interaction potential (9) (grey line) along with the instantaneous dimer length  $y(t)$  (grey dot).

$W(y)$  for  $y \approx L/2$ . However, the non-convexity of  $W(y)$  for  $y$ -values around  $y = \Delta = 0.26L$  allows the dimer to be eventually compressed to about  $L/4$  in length, and to maintain this “metastable” state for almost the complete second half of the driving period. During this phase, the dimer is trapped motionless in a minimum of the rocking potential  $U(x) - xf(t)$ . At about  $6\tau/8$ , when the left potential barrier of the minimum is nearly balanced by the external driving (although the minimum actually never disappears because the driving amplitude  $A$  is smaller than unity), the dimer starts to relaxate back to its equilibrium length  $y = L/2$  by way of “pushing the left monomer over the barrier”. In this manner, the dimer reaches its initial configuration, but with the center being shifted by  $n = 1$  spatial period to the right after  $m = 1$  cycle of the driving, resulting in  $v = +1$ .

From these observations we get an intuitive idea, in addition to the formal arguments of Sec. IV, of why non-convexities in the interaction potential are necessary for spontaneous symmetry breaking. They promote the existence of a “metastable” dimer state with dynamical behavior different from that of the equilibrium configuration. The dimer motion in the periodic potential landscape under the action of the external driving induces periodic transitions between that “metastable” state and the equilibrium configuration, associated with distinct

phases in the dimer motion and thus resulting in an overall symmetry breaking behavior. The above example has been chosen to most clearly illustrate this mechanism, as the specific parameter values give rise to an equilibrium configuration with practically “free” motion of the dimer’s center, whereas in its “metastable” state, the dimer is trapped motionless by the potential landscape. Such a clear-cut distinction between the two states is, however, not necessarily required. Figure 3 shows that spontaneous symmetry breaking occurs in quite large parameter regions, where the “metastable” state is “sufficiently different” from the equilibrium configuration of the dimer.

From our discussion so far, it is evident that average dimer velocities larger in modulus than  $|v| = 1$  should be observable. For instance, for slower driving (smaller  $\omega$ ) the dimer may be able to travel several spatial periods during the first half of the driving cycle, while it gets trapped during the second half of the cycle. Indeed, dimer velocities with  $v = \pm 2$  are present in the black regions of Fig. 3a for small  $\omega$  and small  $A$  values (in Fig. 3, the information on the actual value of non-vanishing average velocities in the black regions is not included though). Likewise, rational velocities with  $|v| < 1$  can, e.g., be found for fast driving at the edges of the black regions towards large  $\omega$  and  $A$  values.

While these considerations are helpful to gain an intuitive picture of what is going on, they obviously do not prove that a specific symmetry breaking solution is dynamically stable (an attractor) and that, besides its twin brother with opposite velocity, no other stable solutions exist. Any such “more rigorous” reasoning would have to depend on the precise quantitative values of all model parameters and thus seems almost impossible.

### C. Generalizations

We finally point out that the specific shape of the interaction potential is not crucial for the existence of spontaneous symmetry breaking, as long as it is non-convex. For instance, we have found spontaneous symmetry breaking attractors for various modifications of (9), including the obvious situation where it has a second minimum, and also the “extreme” case of an “almost convex” potential with a curvature that is positive everywhere except near the equilibrium length  $y \approx L/2$ . Moreover, spontaneous symmetry breaking is also supported by completely different non-convex interaction potentials.

As a specific example, we now turn to our numerical results for the Lennard-Jones potential (8), see also Fig. 2a. For large distances  $y = x_1 - x_2$  of the monomers, their interaction becomes negligibly small. As expected, we found numerically that in this case each monomer exhibits a periodic back-and-forth motion in the long time limit and thus the velocity  $v$  from (13) vanishes. Since these solutions are of little interest, we hence-

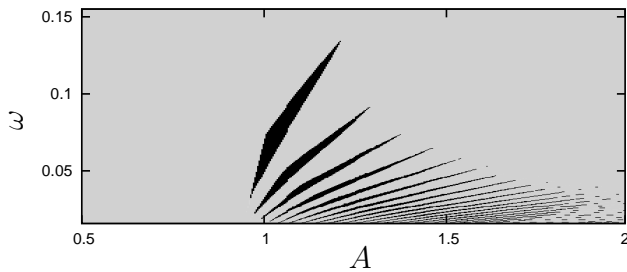


FIG. 5: Same as Fig. 3a but for the Lennard-Jones interaction potential (8) with  $\lambda = 1.25 L$ . Only attractors that can be reached by dimers initially close to their equilibrium lengths are shown, see text.

forth use only initial conditions such that the dimer length is initially close to the equilibrium length  $\lambda$  of the potential (8). More precisely, we only considered  $y(0) \in [0.9 \cdot \lambda, 1.3 \cdot \lambda]$  and observed that the distance  $y(t)$  always remained reasonably small to consider the dimer as “not dissociated” (a rigorous dissociation criterion for the potential (8) seems hard to define). The so obtained numerical results are qualitatively very similar to those for the quartic potential (9), although the quantitative details are different. As an example, Fig. 5 depicts our findings for the Lennard-Jones potential (8) corresponding to those from Fig. 3a for the quartic potential (9). In particular, we recover spontaneous symmetry breaking within a quite notable parameter range. The first main differences compared to the quartic potential is that we did not find coexistence of solutions with  $v = 0$  and  $v \neq 0$ . The second main difference is that all the spontaneous symmetry breaking solutions that we found exhibited the specific velocities  $v = \pm 1$  for all the parameters that we tested.

## VII. GIANT DIFFUSION

We still focus on the unbiased ( $F = 0$ ) dynamics (1)-(4), but now consider finite noise strengths ( $T > 0$ ), implying  $v = 0$  for all model parameters and all initial conditions (see Sec. III). The reason is that any attractor of the deterministic dynamics – in particular those giving rise to spontaneous symmetry breaking – now becomes metastable due to noise induced transitions between them. While the velocity (13) is thus trivial, the quantity of foremost interest is now the diffusion constant (14).

For large noise ( $T \gg 1$ ) in (1)-(5), the effects of the “substrate potential”  $U(x)$  become negligible, hence the diffusion asymptotically approaches the value for the “free” thermal diffusion of the dimer, namely  $D = k_B T / 2\eta$ .

Much more interesting is the opposite asymptotics of small  $T$ , specifically in the case of spontaneously broken symmetry without coexisting deterministic solutions with  $v = 0$ , as exemplified by the black islands in Figs.

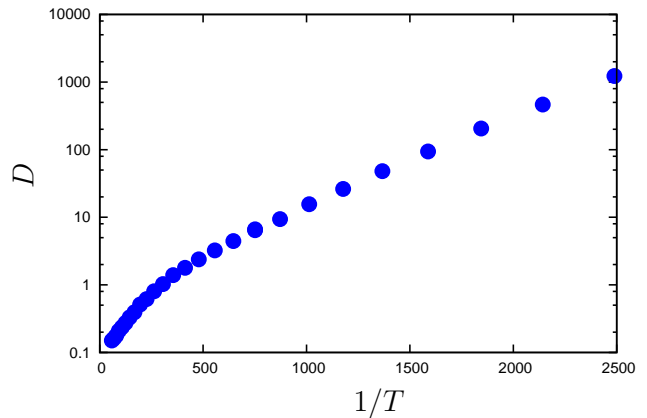


FIG. 6: (Color online) Arrhenius plot (logarithm of  $D$  versus  $1/T$ ) of the diffusion coefficient (14) by numerically solving the unbiased ( $F = 0$ ) dynamics (11), (12) with quartic interaction potential (9) and the specific parameter values indicated by the “x” symbol in Fig. 3a, i.e.  $\omega = 0.11$ ,  $a = 0.95$  and all remaining parameters as in Fig. 3a.

3 and 5. Focusing on this case, a solution  $x_i(t)$  of the noisy dynamics (1)-(4) closely follows most of the time either a deterministic solution exhibiting  $v > 0$  or its twin brother with  $v < 0$ , switching between them every now and then by way of noise activated transitions. For sufficiently weak noise, these transitions become very rare events and are captured very well by a rate process with a certain transition rate  $k$ . A similar calculation as in Ref. [81] then yields for the diffusion coefficient (14) the result

$$D = \frac{L^2}{2\tau^2 k}. \quad (24)$$

The transition rate itself is of the usual Arrhenius-form

$$k = \nu_0 \exp\{-\Delta\phi/T\} \quad (25)$$

with a  $T$ -independent generalized activation energy  $\Delta\phi$  [73] and an “attempt frequency”  $\nu_0$  with a rather weak  $T$ -dependence (at most algebraic). Combining (24) and (25), we thus arrive at the analytical prediction [82] of an extremely strongly diverging diffusion coefficient for asymptotically weak noise strengths  $T$  (essential singularity). The numerical findings in Fig. 6 confirm this prediction very well.

## VIII. ABSOLUTE NEGATIVE MOBILITY

As before, we consider the dynamics (1)-(4) with  $T > 0$ , but now also in the presence of a non-vanishing static bias  $F$ . For symmetry reasons (see Sec. III) we henceforth focus on  $F > 0$ . Our main question is: how does the unperturbed velocity ( $v = 0$  for  $F = 0$ ) respond to a perturbation  $F > 0$ , and, in particular, is it possible to obtain absolute negative mobility, i.e.  $v < 0$ ?

To be specific, we revisit the deterministic ( $T = 0$ ) and unbiased ( $F = 0$ ) dynamics (11), (12) for the quartic potential (9), resulting in the velocity diagram from Fig. 3a. We recall that every black island in this figure indicates the coexistence of two symmetric deterministic attractors, one with  $v > 0$  and the other with  $v < 0$ , and that all solutions (for arbitrary initial conditions) approach one of these two attractors in the long time limit, i.e. all solutions exhibit either  $v > 0$  or  $v < 0$ . As soon as  $F > 0$ , the symmetry of the system is broken and hence the degeneracy of the  $v \neq 0$  solutions lifted. Accordingly, by gradually increasing  $F$ , the “island” in parameter space describing solutions with  $v > 0$  will start to differ more and more from the  $v < 0$  “island”. Every subset of the latter island with  $v < 0$  which is located “outside” of the  $v > 0$  island is clearly a quite promising candidate for absolute negative mobility at finite (sufficiently small)  $T$ . Fig. 7a confirms that such subsets indeed exist and Figs. 7b,c show that they indeed give rise to absolute negative mobility.

By comparing Fig. 7a with Fig. 3a we see that the degeneracy of the  $v > 0$  and  $v < 0$  solutions is lifted by displacements of the red  $v > 0$  “islands” toward larger  $A$  and  $\omega$  values and of the cyan  $v < 0$  “islands” toward smaller  $A$  and  $\omega$  values. While the impact of a change in the driving amplitude  $A$  on a specific solution and its stability is hard to grasp intuitively [83], the existence of a “purely cyan stripe” outside the border of any “red island” toward smaller frequencies  $\omega$  can be understood as follows: In the unbiased case ( $F = 0$ ) from Fig. 3a, the lower border of an island indicates that solutions with  $v \neq 0$  will cease to exist (become unstable) upon further decreasing the driving frequency  $\omega$ . Roughly speaking, the driving thus becomes “too slow” compared to the “eigenspeed” of the solutions, i.e. they are unable to synchronize with the imposed temporal periodicity of the driving. Moreover, if a small bias  $F > 0$  is switched on, it is quite plausible to expect that the intrinsic “eigenspeed” will decrease for solutions traveling “uphill” (against the force  $F$ ), and increase for those traveling downhill. As a consequence, at the lower border of an island in Fig. 3a, those solutions with  $v < 0$  should survive and those with  $v > 0$  disappear when a small  $F > 0$  is switched on, in agreement with Fig. 7a.

Upon further increasing  $F$ , one expects that the cyan and red islands in Fig. 7a change not only their positions, but also their shapes and in particular their areas, and that for sufficiently large  $F$ , the cyan islands will completely disappear. Likewise, with increasing noise strength  $T$ , one expects that the original deterministic solutions become less and less relevant. Indeed, for  $T \rightarrow \infty$  the effects of the substrate potential  $U(x)$  in (4) become negligible, yielding for the velocity (13) the trivial result  $v = F/\eta$ . These quite plausible qualitative features are indeed confirmed by our numerical results for a representative example in Fig. 7c.

Turning to the Lennard-Jones potential (8), it is quite plausible and can be confirmed by more detailed calcu-

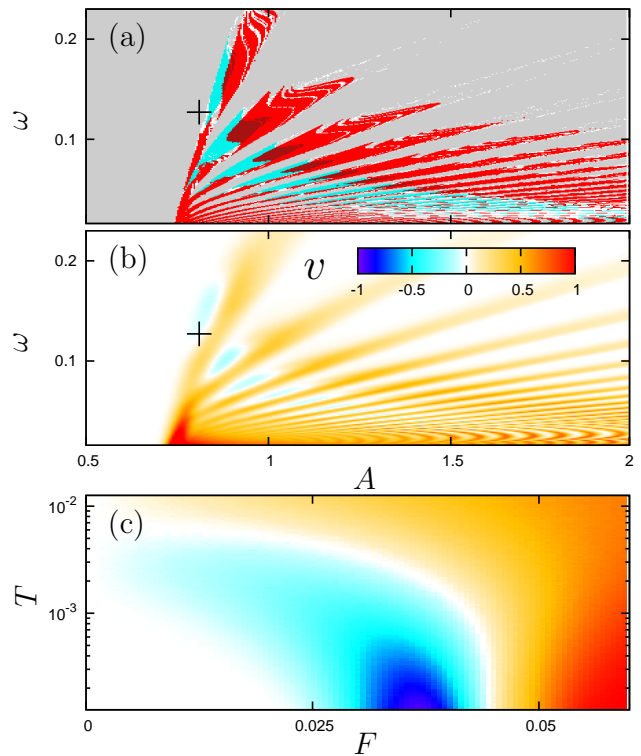


FIG. 7: (Color) (a): Same as Fig. 3a, but for a finite bias  $F = 0.01$ . Red: Velocities  $v > 0$ . Cyan: Velocities  $v < 0$ . Red and cyan overlapping: Coexistence of solutions with opposite average velocities. Grey: Velocities  $v = 0$ . Coexistence of  $v \neq 0$  and  $v = 0$  is restricted to negligibly small parameter regions and is not shown in this figure. (b): Same as in (a) but for a finite noise strength  $T = 0.005$ . The value of the velocity  $v$  from (13) is independent of the initial conditions and indicated by the color code. In particular, blue regions correspond to absolute negative mobility ( $v < 0$  for  $F > 0$ ). (c) Dependence of the velocity  $v$  on the bias  $F$  and the noise strength  $T$  for fixed driving parameters as indicated by the black “+” in (a) and (b).

lations that any solution of (1) with  $T > 0$  results in a dissociation of the dimer in the long run, and that this implies  $v > 0$  for all  $F > 0$ . However, for small  $T$  and  $F$ , the lifetime of the dimer is still very large, and restricting the time-average of the velocity in (13) accordingly, the same qualitative features as in Fig. 7 are recovered (not shown). Fig. 8 exemplifies a typical solution exhibiting absolute negative mobility during the extremely long initial time-period before the dimer dissociates. The very long life-time of the dimer can be understood intuitively as follows: As a relict of the underlying (dynamically stable) symmetry-breaking attractor, the dimer length never increases notably beyond 2 during the motion shown in Fig. 8. The binding energy of the dimer at that length is still  $\mathcal{O}(10^{-1})$  (see Fig. 2b) and thus much larger than the thermal energy corresponding to  $T = 0.001$ , so that noise-induced dissociation events are extremely rare.



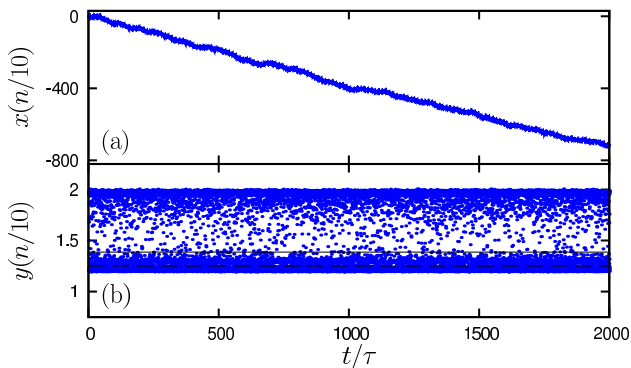


FIG. 8: (Color online) (a) Center of mass  $x(t)$  from (10) for the dynamics (11), (12) with Lennard-Jones interaction potential (9). Remaining parameters:  $A = 1$ ,  $\omega = 0.06$ ,  $T = 0.001$ ,  $F = 0.01$ . (b) Dimer length  $y(t)$  at the time points  $t = n/10$  for  $n = 0, 1, \dots, 20000$ .

## IX. OUTLOOK ON HIGHER DIMENSIONAL MODELS

In this section we address the motion of two coupled particles in 2- or 3-dimensional periodic potentials, e.g. on a crystal surface, in a lattice of optical or magnetic traps etc., see also Sec. I. A particularly interesting special case arises for systems with a pronounced anisotropy, causing a strong preferential direction (“easy axis”) for the dimer motion and orientation, as exemplified with Fig. 1.

Focusing on this case, the one-dimensional model (1)-(4) still describes such systems reasonably well, especially with the following modification: The main effect of the omitted additional dimensions is that the dimer may “turn around” by  $180^\circ$ , albeit with a very low probability per time unit (due to the strong anisotropy). This feature can be effectively incorporated into the model (1)-(4) by choosing an interaction potential  $W(y)$  which exhibits two minima, one at a positive and one at a negative  $y$ -value, separated by a “high” energy barrier at  $y = 0$  (to guarantee “rare” transitions). In other words, a sign change of  $x_1 - x_2 = y$  (cf. Eq. (10)) does not mean that the two particle pass “through” each other, but rather that they perform a rotation. In contrast to our convention at the end of Sec. II, we furthermore restrict ourselves to “physically realistic” interactions, depending only on the absolute particle distance and thus satisfying

$$W(-y) = W(y). \quad (26)$$

In other words,  $W(y)$  exhibits a symmetric double well structure and thus is always a non-convex potential.

Numerically, we found that effectively one-dimensional models of the above type reproduce all the main effects from Secs. VI-VIII. Essentially, the reason is that once the solutions of a model as specified in Sec. II are known, the solutions of the same model but with

$W(y) \mapsto W(y + L)$  follow immediately and the resulting velocities and diffusion coefficients remain unchanged. Hence, our present double well potential  $W(y)$  with a barrier at  $y = 0$  can be readily shifted by any integer multiple of  $L$  “to the right” until it becomes similar to the one of the previously considered interaction potentials (see Sec. VI.C).

More generally, also dimers consisting of non-identical particles can be approximated by an effectively one-dimensional model analogous to (1)-(4), except that the friction coefficients  $\eta$  in (1) may now be different for the two particles, and similarly for the “coupling strengths” to the forces  $F$ ,  $f(t)$  and the substrate potentials  $U(x)$ . As a consequence, one can show that the system satisfies only a weaker symmetry property than the one from Sec. III. Accordingly, a spontaneous breaking of this symmetry is in many cases rather trivial: Namely, the dimer exhibits a standard ratchet effect since the two particles are different and never actually exchange their positions during their time-evolution [33, 46, 47]. Considerably less trivial at first glance is the occurrence of giant diffusion and absolute negative mobility in such systems. But given our previous discussions in Secs. VII and VIII, these effects are, of course, immediate consequences of the spontaneous symmetry breaking.

## X. CONCLUSIONS

We considered a very simple “minimal” model arising in a large variety of different situations (see Sec. I): Two coupled overdamped Brownian particles moving along a periodic substrate potential in one or more dimensions. In spite of the fact that the particles are identical and the substrate spatially symmetric, a sinusoidal external driving may lead to spontaneous symmetry breaking in the form of a permanent directed motion of the dimer (spontaneous transport, see Sec. V) in the deterministic limit ( $T = 0$ ). Thermal noise ( $T > 0$ ) restores ergodicity and thus zero net velocity, but entails arbitrarily fast diffusion of the dimer for asymptotically small temperatures  $T$  (Sec. VII). Moreover, for small but finite  $T$  the dimer responds to a static bias force with motion opposite to that force (absolute negative mobility, see Sec. VIII). As proven in Sec. IV, the key requirement for all these effects is a non-convex interaction potential of the two particles (Sec. V).

Directed transport induced by spontaneous symmetry breaking as a collective effect of infinitely many particles far from equilibrium has been observed before, e.g., in Refs. [18, 64, 65, 68]. These systems and also the basic physical mechanism are quite different from our present case (Sec. VI.B). Spontaneous symmetry breaking induced transport for periodically driven, underdamped (finite inertia) systems [69–72] is, mathematically speaking, closer related to our case (both types of dynamics are two-dimensional, dissipative, and non-autonomous), while the underlying physical systems (Sec. I) are en-

tirely different.

Diffusion enhancement phenomena are well established already for a single overdamped particle under the influence of an unbiased, temporally periodic driving force [60–62]. But a diverging diffusion coefficient for asymptotically weak noise has been reported for the first time only very recently in [82]. In particular, we remark that, unlike in [60–62], in our present case, the parameter space of diffusion enhancement does not approach a set of measure zero for asymptotically weak noise.

Absolute negative mobility has been reported in a considerable variety of experimental systems and theoretical models by now, see [54] for a recent review. Within the realm of classical models (no quantum effects), it has been observed for the first time as a collective effect of infinitely many interacting particles under far from equilibrium conditions [74]. Later, this model was successfully reduced down to 3 interacting particles [75]. Although this model is very different from ours, the present results for two interacting particles may be seen as the next and ultimate reduction step, since, as demonstrated in [71], a single overdamped particle in one dimension cannot exhibit absolute negative mobility.

A somewhat similar stochastic dynamics of two coupled Josephson junctions exhibiting absolute negative mobility has recently been studied in Ref. [29]. This model is mathematically equivalent to the overdamped dynamics of two coupled particles. However, it exhibits certain features which are very different from our present model: (i) The two particles are not identical in all respects; (ii) The interaction forces cannot be derived from an interaction potential. Moreover, they are spatially periodic, i.e. not approaching zero for large particle distances. Besides those differences in the considered model,

also the basic mechanism generating absolute negative mobility is very different.

Further, mathematically somewhat similar but physically completely different systems exhibiting absolute negative mobility are (i) a single underdamped (finite inertia) particle in one dimension [71, 72, 76], (ii) an overdamped particle on a one-dimensional “meandering” state space [54, 77] (iii) an overdamped particle in 2 dimensions [78], and (iv) a single particle in one dimension with some kind of “internal degree of freedom” [79]. The recent work [52] may be considered as an extension of the above mentioned system class (i) to the case of two coupled underdamped particles.

In the context of nano-friction experiments by atomic force microscope (AFM), it has been reported [84] that an external time-periodic forcing may result in unmeasurably small sliding friction forces (so-called superlubricity). Given that dimer models are well established to describe such systems [22–25], our present results predict the possibility of an even more astonishing effect, namely sliding friction with negative sign, i.e. opposite to the direction of the pulling velocity.

For colloidal particles in magnetic or optical traps [20, 21], an effective “bias” force is often generated by moving the traps with respect to the ambient fluid and then going over into the comoving reference frame. Along the lines of our present work, it might be possible to make colloidal doublets [19] move oppositely to the moving (and usually “entraining”) traps.

This work was supported by Deutsche Forschungsgemeinschaft under RE1344/5-1 and SFB 613, and by the ESF program FANAS (collaborative research project Nanoparma-07-FANAS-FP-009, RE1344/6-1).

- 
- [1] G. Boisvert, and L. J. Lewis, *Phys. Rev. B* **56**, 7643 (1997).
  - [2] X. R. Qin, B. S. Swartzentruber, and M. G. Lagally, *Phys. Rev. Lett.* **85**, 3660 (2000).
  - [3] E. Pijper, and A. Fasolino, *J. Chem. Phys.* **126**, 014708 (2007).
  - [4] O. M. Braun, R. Ferrando, and G. E. Tommei, *Phys. Rev. E* **68**, 051101 (2003).
  - [5] C. Fusco and A. Fasolino, *Thin Solid Films* **428**, 34 (2003).
  - [6] E. Heinsalu, M. Patriarca, and F. Marchesoni, *Phys. Rev. E* **77**, 021129 (2008).
  - [7] A. H. Romero, A. M. Lacasta, and J. M. Sancho, *Phys. Rev. E* **69**, 051105 (2004).
  - [8] E. Pijper and A. Fasolino, *Phys. Rev. B* **72**, 165328 (2005).
  - [9] A. Ajdari, *J. Phys. I France* **4**, 1577 (1994).
  - [10] C. S. Peskin, G. Oster, *Biophys. J.* **68**, 202, (1995).
  - [11] A. Mogliner, M. Mangel, R. J. Baskin, *Phys. Lett. A* **237**, 297 (1998).
  - [12] R. D. Astumian, I. Derényi, *Biophys. J.* **77**, 993 (1999); R. D. Astumian, *Phil. Trans. R. Soc. London B* **355**, 511 (2000).
  - [13] G. N. Stratopoulos, T. E. Dialynas, G. Tsironis, *Phys. Lett. A* **252**, 151 (1999).
  - [14] T. C. Elston, C. S. Peskin, *SIAM J. Appl. Math.* **60**, 842 (2000); T. C. Elston, D. You, C. S. Peskin, *SIAM J. Appl. Math.* **61**, 776 (2000).
  - [15] Y. Li, X. Wu, Y. Zhou, *Mod. Phys. Lett. B* **14**, 479 (2000).
  - [16] I. Derényi and T. Vicsek, *Proc. Natl. Acad. Sci. U. S. A.* **93**, 6775 (1996).
  - [17] S. Klumpp, A. Mielke, and C. Wald, *Phys. Rev. E* **63**, 031914 (2001).
  - [18] F. Jülicher, A. Ajdari, and J. Prost, *Rev. Mod. Phys.* **69**, 1269 (1997).
  - [19] P. Tierno, R. Golestanian, I. Pagonabarraga, and F. Sagués, *Phys. Rev. Lett.* **101**, 218304 (2008); P. Tierno et al., *Phys. Rev. E* **81**, 011402 (2010).
  - [20] P. Tierno, F. Sagués, T.H. Johansen, and T.M Fischer, *Phys. Chem. Chem. Phys.* **11**, 9615 (2009); P. Tierno, P. Reimann, T.H. Johansen, and F. Sagués, *Phys. Rev. Lett.* **105**, 230602 (2010).
  - [21] K. Mangold, P. Leiderer, and C. Bechinger, *Phys. Rev.*

- Lett. **90**, 158302 (2003); P.T. Korda, M.B. Taylor, and D.G. Grier, Phys. Rev. Lett. **89**, 128301 (2002)
- [22] M. Tiwari, S. Goncalves, and V. M. Kenkre, Eur. Phys. J. B **62**, 459 (2008).
- [23] S. Goncalves, C. Fusco, A. R. Bishop, and V. M. Kenkre, Phys. Rev. B **72**, 195418 (2005).
- [24] S. Goncalves, V. M. Kenkre, and A. R. Bishop, Phys. Rev. B **70**, 195415 (2004).
- [25] S. Maier, Y. Sang, T. Filleter, M. Grant, R. Bennewitz, E. Gnecco, and E. Meyer, Phys. Rev. B **72**, 245418 (2005).
- [26] H. D. Vollmer, Z. Phys. B Con. Mat. **33**, 103 (1979).
- [27] M. Patriarca, and P. Szelestey, Act. Phys. Pol. B **36**, 1745 (2005).
- [28] I. Zapata, R. Bartussek, F. Sols, and P. Hänggi, Phys. Rev. Lett. **77**, 2292 (1996); A. Sterck, R. Kleiner, and D. Koelle, Phys. Rev. Lett. **95**, 177006 (2005); A. Sterck, D. Koelle, and R. Kleiner, Phys. Rev. Lett. **103**, 047001 (2009)
- [29] M. Januszewski and J. Luczka, Phys. Rev. E **83**, 051117 (2011)
- [30] T. E. Dyalnas, G. Tsironis, Phys. Lett. A **218**, 292 (1996)
- [31] T. E. Dyalnas, K. Lindenberg, G. P. Tsironis, Phys. Rev. E **56**, 3976 (1997).
- [32] S. Cilla, L. M. Floria, Physica D **113**, 157 (1998); S. Cilla, L. M. Floria, Il Nuovo Cimento D **20**, 1761 (1998)
- [33] S. Cilla, F. Falo, and L. M. Floria, Phys. Rev. E **63**, 031110 (2001).
- [34] E. M. Craig, M. J. Zuckermann, and H. Linke, Phys. Rev. E **73**, 051106 (2006).
- [35] D. Dan, A. M. Jayannavar, and G. I. Menon, Physica A **318**, 40 (2003).
- [36] J. A. Fornes, J. Colloid Interf. Sci. **341**, 376 (2010).
- [37] U. E. Vincent, A. Kenfack, D. V. Senthilkumar, D. Mayer, and J. Kurths, Phys. Rev. E **82**, 046208 (2010); U. E. Vincent, O. I. Olusola, D. Mayer, and P. V. E. McClintock, J. Phys. A **43**, 165101 (2010).
- [38] Y. A. Makhnovskii, V. M. Rozenbaum, D.-Y. Yang, and S. H. Lin, J. Chem. Phys. **130**, 164101 (2009).
- [39] J. Mateos, Fluct. Noise Lett. **4**, L161 (2004).
- [40] J. L. Mateos and F. R. Alatrisme, Chaos **18** (2008).
- [41] K. V. Kumar, S. Ramaswamy, and M. Rao, Phys. Rev. E **77**, 020102(R) (2008).
- [42] J. Menche and L. Schimansky-Geier, Phys. Lett. A **359**, 90 (2006).
- [43] A. Pototsky, N. B. Janson, F. Marchesoni, and S. Savel'ev, Europhys. Lett. **88**, 30003 (2009).
- [44] A. Pototsky, F. Marchesoni, and S. E. Savel'ev, Phys. Rev. E **81**, 031114 (2010).
- [45] R. Retkute and J. P. Gleeson, Fluct. Noise Lett. **6**, L263 (2006).
- [46] S. von Gehlen, M. Evstigneev, and P. Reimann, Phys. Rev. E **77**, 031136 (2008).
- [47] S. von Gehlen, M. Evstigneev, and P. Reimann, Phys. Rev. E **79**, 031114 (2009).
- [48] M. Evstigneev, S. von Gehlen, and P. Reimann, Phys. Rev. E **79**, 011116 (2009).
- [49] C. Fusco and A. Fasolino, Chem. Phys. Chem. **6**, 1749 (2005).
- [50] J. Bammert, S. Schreiber, and W. Zimmermann, Phys. Rev. E **77**, 042102 (2008).
- [51] D. Hennig, S. Martens, and S. Fugmann, Phys. Rev. E **78**, 011104 (2008).
- [52] C. Mulhern and D. Hennig, Phys. Rev. E **84**, 036202 (2011).
- [53] D. Denisov, Phys. Lett. A **296**, 197 (2002).
- [54] R. Eichhorn, P. Reimann, B. Cleuren, and C. Van den Broeck, Chaos **15**, 026113 (2005).
- [55] A. A. Middleton and D. S. Fisher, Phys. Rev. Lett. **66**, 92 (1991).
- [56] A. A. Middleton, Phys. Rev. Lett. **68**, 670 (1992).
- [57] A. A. Middleton and D. S. Fisher, Phys. Rev. B **47**, 3530 (1993).
- [58] L. M. Floría and J. J. Mazo, Adv. Phys. **45**, 505 (1996).
- [59] C. Baesens and R. S. MacKay, Nonlinearity **11**, 949 (1998).
- [60] H. Gang, A. Daffertshofer, and H. Haken, Phys. Rev. Lett. **76** 4874 (1996).
- [61] M. Schreier, P. Reimann, P. Hänggi, and E. Pollak, Europhys. Lett. **44**, 416 (1998).
- [62] D. Reguera, P. Reimann, P. Hänggi, and J. M. Rubi, Europhys. Lett. **57**, 644 (2002).
- [63] S. H. Strogatz, *Nonlinear dynamics and chaos*. Perseus Books, Reading, Mass., 1998.
- [64] F. Jülicher and J. Prost, Phys. Rev. Lett. **75**, 2618 (1995).
- [65] M. Badoual, F. Jülicher, and J. Prost, Proc. Natl. Acad. Sci. U. S. A. **99**, 6696 (2002).
- [66] S. Endow and H. Higuchi, Nature **406**, 913 (2000); M. Badoual, F. Jülicher, and J. Prost, Proc. Natl. Acad. Sci. U. S. A. **99**, 6696 (2002).
- [67] M. Bishop, M. Derosa, and J. Lalli, J. Stat. Phys. **25**, 229 (1981); A. M. Bazhenov and D. M. Heyes, J. Chem. Phys. **92**, 1106 (1990); S. Lepri, P. Sandri, and A. Politi, Eur. Phys. J. B **47**, 549 (2005).
- [68] P. Reimann, R. Kawai, C. Van den Broeck, and P. Hänggi, Europhys. Lett. **45**, 545 (1999); P. Reimann, C. Van den Broeck, and R. Kawai, Phys. Rev. E **60**, 6402 (1999).
- [69] A. Barone, *Physics and Applications of the Josephson Effect*. John Wiley and Sons, Inc., New York, 1982.
- [70] R. L. Kautz, Rep. Prog. Phys. **59**, 935 (1996).
- [71] D. Speer, R. Eichhorn, and P. Reimann, Europhys. Lett. **79**, 10005 (2007); D. Speer, R. Eichhorn, and P. Reimann, Phys. Rev. E **76**, 051110 (2007).
- [72] J. Nagel, D. Speer, T. Gaber, A. Sterck, R. Eichhorn, P. Reimann, K. Ilin, M. Siegel, D. Koelle, and R. Kleiner, Phys. Rev. Lett. **100**, 217001 (2008).
- [73] J. Lehmann, P. Reimann, and P. Hänggi, phys. stat. sol. (b) **237**, 53 (2003).
- [74] P. Reimann, R. Kawai, C. Van den Broeck, and P. Hänggi, Europhys. Lett. **45**, 545 (1999); P. Reimann, C. Van den Broeck, and R. Kawai, Phys. Rev. E **60**, 6402 (1999); J. Buceta, J. M. Parrondo, C. Van den Broeck, and F. J. de la Rubia, Phys. Rev. E **61**, 6287 (2000); C. Van den Broeck, I. Bena, P. Reimann, and J. Lehmann, Ann. Phys. (Leipzig) **9**, 713 (2000); S. E. Mangioni, R. R. Deza, and H. S. Wio, Phys. Rev. E **63**, 041115 (2001).
- [75] C. Van den Broeck, B. Cleuren, and R. Kawai, Int. J. Mod. Phys. C **13**, 1195 (2002).
- [76] L. Machura, M. Kostur, P. Talkner, J. Luczka and P. Hänggi, Phys. Rev. Lett. **98**, 040601 (2007); M. Kostur, L. Machura, P. Talkner, P. Hänggi and J. Luczka, Phys. Rev. B **77**, 104509 (2008); M. Kostur, J. Luczka and P. Hänggi, Phys. Rev. E **80**, 051121 (2009).
- [77] R. Eichhorn and P. Reimann, Phys. Rev. E **70**,

- 035106(R) (2004); R. Eichhorn and P. Reimann, Europhys. Lett. **69**, 517 (2005).
- [78] R. Eichhorn, P. Reimann and P. Hänggi, Phys. Rev. Lett. **88**, 190601 (2002); R. Eichhorn, P. Reimann and P. Hänggi, Phys. Rev. E **66**, 066132 (2002); R. Eichhorn, P. Reimann and P. Hänggi, Physica A **325**, 101 (2003); B. Cleuren and C. Van den Broeck, Phys. Rev. E **67**, 055101(R) (2003); A. Ros, R. Eichhorn, J. Regtmeier, T. T. Duong, P. Reimann and D. Anselmetti, Nature **436**, 928 (2005); R. Eichhorn, A. Ros, J. Regtmeier, T. T. Duong, P. Reimann and D. Anselmetti, Eur. Phys. J. Special Topics **143**, 159 (2007); R. Eichhorn, J. Regtmeier, D. Anselmetti, and P. Reimann, Soft Matter **6**, 1858 (2010).
- [79] B. Cleuren and C. Van den Broeck, Phys. Rev. E **65**, 030101(R) (2002); B. Jiménez de Cisneros, P. Reimann and J. M. R. Parrondo, Europhys. Lett. **64**, 599 (2003); A. Haljas, R. Mankin, A. Sauga, and E. Reiter, Phys. Rev. E **70**, 041107 (2004).
- [80] O. Sandre, L. Gorre-Talini, A. Ajdari, J. Prost, P. Silberzan, Phys. Rev. E **60**, 2964 (1999).
- [81] M. Schell, S. Fraser, and R. Kapral, Phys. Rev. A **26**, 504 (1982); P. Reimann and C. Van den Broeck, Physica D **75**, 509 (1994); B. Lindner and E. M. Nicola, Phys. Rev. Lett. **101**, 190603 (2008).
- [82] D. Speer, R. Eichhorn, and P. Reimann, EPL **97**, 60004 (2012).
- [83] D. Speer, PhD-Thesis, Bielefeld 2011, <http://bieson.ub.uni-bielefeld.de/volltexte/2011/1848/>
- [84] A. Socoliuc et al., Science **313**, 207 (2006)